Ferroelectric Materials

DOI: 10.1002/anie.200703146

A Pure Bismuth A Site Polar Perovskite Synthesized at Ambient Pressure**

*Craig A. Bridges, Mathieu Allix, Matthew R. Suchomel, Xiaojun Kuang, Iasmi Sterianou, Derek C. Sinclair, and Matthew J. Rosseinsky**

The perovskite oxide lead zirconate titanate (PZT) has produced an entire set of technologies (actuators, sensors, transducers)[1] based on the remarkable electromechanical and electrical properties associated with the morphotropic phase boundary (MPB), which is formed by doping antiferroelectric $PbZrO_3$ with ferroelectric (ca. 48%) $PbTiO_3$ and which occurs for the coexistence of tetragonal (*P*4*mm* symmetry F_T), monoclinic (*Cm* symmetry F_M), and rhombohedral (*R*3*c* symmetry F_R) polar distortions of the perovskite structure.[2] These distortions arise predominantly through ferroelectric coupling of the locally acentric environment of the Pb^{2+} ion produced by the stereochemically active $6s^2$ electron pair. However, concern about the environmental impact of Pb-based systems has spurred considerable interest in the discovery of Pb-free ferroelectric materials.[3–5] To date, a significant obstacle to identifying PZT replacements has been the difficulty in finding materials with equivalent figures of merit but without the powerful structural influence of Pb^{2+}; the recently discovered (K,Na)NbO_3-based systems are promising candidates.[5] The presence of the $6s^2$ inert pair of electrons marks the Bi^{3+} ion as a suitable replacement for the Pb^{2+} ion. Reports on Bi- and Pb-based solid solutions, such as the $PbTiO_3$/$BiScO_3$ system,[6] have demonstrated the possibility of superior electromechanical responses in compositions with reduced Pb content. However, efforts to identify promising candidates based entirely on Bi have proven less successful. Herein, we report the synthesis at ambient pressure of polar perovskites containing solely Bi on the A site of the ABO_3 perovskite structure, which highlights a new strategy for targeting ambient-pressure Pb-free compositions.

Few perovskites with only Bi^{3+} ions occupying the A site are stable under ambient-pressure, bulk-synthesis conditions; $BiFeO_3$ and $Bi_2Mn_{4/3}Ni_{2/3}O_6$ are the only two reported examples.[7,8] This paucity is ascribed to the small size of the Bi^{3+} ion and the resulting mismatch with the twelve-coordinate A site. The case of $Bi_2Mn_{4/3}Ni_{2/3}O_6$ is instructive; the use of two cations with three valence states (Mn^{3+}, Mn^{4+}, Ni^{2+}) on the B site allows the stabilization of a solid solution between the two end-members $BiMnO_3$ and $BiNiO_3$, neither of which can be formed by ambient-pressure synthesis methods.[9,10,11] The presence of cations of different sizes that either do or do not display Jahn–Teller distortions permits the mean bonding environment at the octahedral B site to relax sufficiently to accommodate the undersized and low-symmetry Bi cation on the A site. This finding suggests that there are "magic" compositions or islands of stability in Bi-based perovskite chemistry that are accessible by expanding the compositional complexity of the B site.

To test this strategy of enhancing Bi perovskite stability by matching the A-site Bi environment to the B-site bonding, we expanded the search for materials with multiple octahedral-site cations to a broader range of metals. Herein, we show that using Ti^{4+} in place of Mn^{4+} ions, Fe^{3+} in place of Mn^{3+} ions, and either of the divalent cations Ni^{2+} or Mg^{2+} leads to the formation of A-site Bi-based polar perovskite compounds that are stable at ambient pressure and which have structures that are distinctly different from that of $Bi_2Mn_{4/3}Ni_{2/3}O_6$. This approach of enhancing perovskite stability by increasing B-site complexity is versatile and promising for the next generation of lead-free ferroelectric materials.

The initial target composition of this investigation, $BiTi_{1/3}Fe_{1/3}Ni_{1/3}O_3$, was selected by direct replacement of the cations in $Bi_2Mn_{4/3}Ni_{2/3}O_6$: Ti^{4+} for Mn^{4+}, Fe^{3+}, for Mn^{3+}, and retention of Ni^{2+}. The outcome of the reaction at this compositional target was multiphase, but it did contain a phase with the perovskite structure. Compositional determination of this perovskite-structure component within the multiphase assembly by EDS (energy-dispersive spectroscopy) in the TEM investigation gave the metal-element ratios of $Bi_{1.0}Ti_{0.385}Fe_{0.235}Ni_{0.36}$. This outcome suggests that the introduction of a d^0 cation changes the optimal multiple-cation stabilizing composition for Bi-based systems from that observed for the all-d^n Mn/Ni B-site occupancy in $Bi_2Mn_{4/3}Ni_{2/3}O_6$.[8] Systematic investigations of different synthetic compositions within the framework of the pseudoternary phase diagram (Figure S1 in the Supporting Information) resulted in the isolation of a pure sample at the composition $BiTi_{3/8}Fe_{2/8}Ni_{3/8}O_3$, which agrees well with the initial perovskite structure cation ratios found by EDS. Subsequent investigations, in which the divalent Ni^{2+} ions were replaced by Mg^{2+} ions, identified an analogous perovskite structure with the EDS-confirmed composition, $BiTi_{3/8}Fe_{2/8}Mg_{3/8}O_3$.

[*] Dr. C. A. Bridges, Dr. M. Allix, Dr. M. R. Suchomel, Dr. X. Kuang, Prof. M. J. Rosseinsky
Department of Chemistry, University of Liverpool
Liverpool L69 7ZD (UK)
Fax: (+44) 151-794-3587
E-mail: m.j.rosseinsky@liv.ac.uk
Homepage: http://www.liv.ac.uk/chemistry/Postgraduate/portfolio.html
I. Sterianou, Dr. D. C. Sinclair
Department of Engineering Materials, University of Sheffield
Sheffield, S1 3JD (UK)

[**] We thank the EPSRC for funding under EPSRC/C511794 and the EU for support of the FAME Network of Excellence.

Supporting information for this article is available on the WWW under http://www.angewandte.org or from the author.

Details of synthesis and characterization are provided in the Supporting Information.

Initial refinements revealed the structures of both materials to be rhombohedral polar perovskites (Figure S2 in the Supporting Information shows the poor fit in the centrosymmmetric space group $R\bar{3}c$). In electroceramics with multiple-cation disorder,[3] crystallographic symmetry descriptions are often problematic. In this case, substantial anisotropic line broadening (see Figure S3 in the Supporting Information) precludes refinement of high-resolution neutron powder diffraction data in $R3c$ with line-broadening appropriate to $R3c$ symmetry. Lowering the structural symmetry to monoclinic Cc with $2/m$ symmetry-strain broadening gives an improved and stable refinement, but the cell metric and atom positions have strong $R3c$ pseudosymmetry, and no extra reflections characteristic of the lower symmetry are observed. Refinement in $R3c$ with $\bar{1}$ symmetry-strain broadening afforded essentially equivalent profile fitting and was thus adopted in preference to the description in the lower-symmetry space group. The significant improvement in the $R3c$ fit stemming from refinement of anisotropic displacement parameters on the Bi and O sites gave a Bi scattering density distribution that was highly elongated perpendicular to the rhombohedral c axis (Figure S4a in the Supporting Information). This situation contrasts with $BiFeO_3$[12] (for which the Bi displacements are essentially isotropic, see Figure S4b in the Supporting Information) but is similar to the Pb displacement parameter observed in F_R-PZT.[13] An equivalent fit to both $BiTi_{3/8}Fe_{2/8}Mg_{3/8}O_3$ and $BiTi_{3/8}Fe_{2/8}Ni_{3/8}O_3$ is achieved using fewer parameters and a physically sensible isotropic displacement parameter by displacing Bi centers onto the general 18f (xyz) position in $R3c$ (Figure 1a). This approach gives a displacement from the threefold axis solely along $\langle 010\rangle$, which is in contrast to the ($xy0$) displacement within the plane found in F_R-PZT. Atom positions from this final structural model (Figure 2) are given in Tables 1 and 2. The average structure refinement in $R3c$ reflects the microstrain apparent in the hkl-dependent broadening through disorder in the local displacement of Bi cations and the occupancy of the octahedral site. If these local displacements were to become ordered over the coherent length for diffraction, extra reflections corresponding to Cc symmetry would appear. The final structural analysis was performed simultaneously against neutron and X-ray data sets for $BiTi_{3/8}Fe_{2/8}Mg_{3/8}O_3$. No evidence was found for a separate Ti position on the octahedral site, and the displacement of the Bi center from its original position on the threefold axis is 0.11 Å. Refinement of $BiTi_{3/8}Fe_{2/8}Ni_{3/8}O_3$ (neutron data only, Figure S5 in the Supporting Information) reveals an almost identical Bi displacement from the threefold axis.

Impedance measurements performed on dense sintered pellets revealed a semiconducting temperature dependence for both $BiTi_{3/8}Fe_{2/8}Ni_{3/8}O_3$ and $BiTi_{3/8}Fe_{2/8}Mg_{3/8}O_3$ (Figure S6 in the Supporting Information). The measured conductivity of the former, with its higher fraction of d^n B-site occupancy, was several orders of magnitude higher than that measured for the Mg^{2+}-based composition

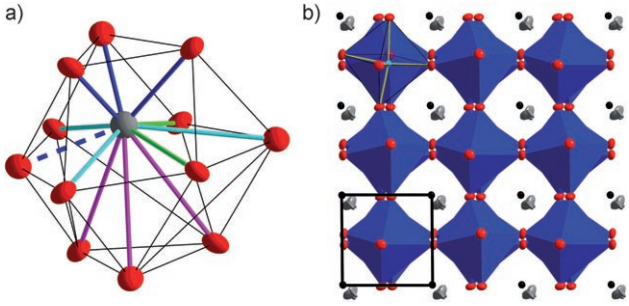

Figure 1. a) The coordination of Bi^{3+} ions on the A site of $BiTi_{3/8}Fe_{2/8}Mg_{3/8}O_3$. Bi^{3+} is predominantly displaced along $[111]_p$ (the c direction of $R3c$) within the cuboctahedron of twelve oxide anions (solid black lines) to form three short Bi–O contacts (blue). In the anisotropic model for Bi displacements (see Figure S4a in the Supporting Information), the ordered static displacement is purely along this direction, with Bi on (0,0,0); there are three longer bonds of 2.527 Å (two shown in green) resulting from the octahedral tilt. In the refined model (Tables 1 and 2), disordered Bi displacements along $\langle 110\rangle_p$ towards one of these three next-nearest oxide neighbors (broken blue line) produce four close Bi–O contacts. b) The BO_6 octahedra (blue) are tilted by equal angles about each of the pseudocubic axes, giving a rotation $\langle\omega\rangle$ about $[111]_p$ of 11.94° ($BiTi_{3/8}Fe_{2/8}Mg_{3/8}O_3$) and 12.21° ($BiTi_{3/8}Fe_{2/8}Ni_{3/8}O_3$; see also Table S2 in the Supporting Information). The A-site displacement (gray ellipsoids) away from the centroid of coordinating O atoms (black spheres) is shown. The B-site displacement along $[111]_p$ is illustrated in the transparent (top left) octahedron and in Figure S10 in the Supporting Information. The pseudocubic unit cell of dimension $a_p \approx 3.8$ Å, to which structural distortions are referred in the text, is shown on the bottom left.

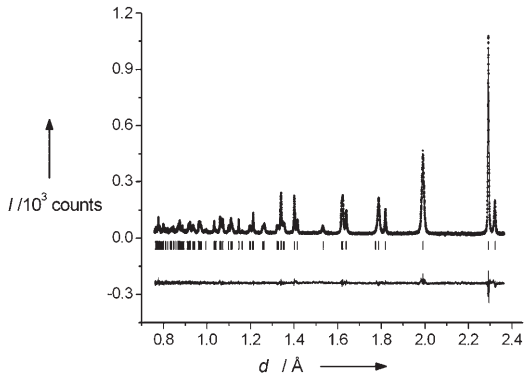

Figure 2. Rietveld refinement for $BiTi_{3/8}Fe_{2/8}Mg_{3/8}O_3$ from powder neutron diffraction data ($\chi = 1.44$, $R_{wp} = 7.59\%$) at room temperature in the $R3c$ space group with $\bar{1}$ microstructure parameters. The data were collected on the HRPD beamline at the ISIS facility.

Table 1: Refined coordinates for $BiTi_{3/8}Fe_{2/8}Ni_{3/8}O_3$.[a]

	x	y	z	U_{iso} [Å^{-2}][b]	Occupancy
Bi	0	0.0207(3)	0	0.0113(2)	$^1/_3$
Ti,Fe,Ni	0	0	0.22215(4)	0.0054(1)	$^3/_8$, $^2/_8$, $^3/_8$
O1	0.44567(8)	0.01593(9)	0.95609(4)	0.0129(2)	1

[a] $a = 5.58471(5)$, $c = 13.8157(2)$ Å, space group $R3c$. $wR_p = 1.16$, $\chi^2 = 2.52$. (Neutron–Polaris beamline) [b] O1 U_{ij} parameters: $U_{11} = 0.0142(2)$, $U_{22} = 0.0122(2)$, $U_{33} = 0.0121(1)$, $U_{12} = 0.0052(2)$, $U_{13} = -0.0014(1)$, $U_{23} = -0.0040(1)$. The quoted O U_{iso} is an equivalent value derived from these ADPs.

Table 2: Refined coordinates for $BiTi_{3/8}Fe_{2/8}Mg_{3/8}O_3$.[a]

	x	*y*	*z*	U_{iso} [Å^{-2}][b]	Occupancy
Bi	0	0.0197(7)	0	0.0163(3)	$^1/_3$
Ti,Fe,Mg	0	0	0.2209(2)	0.0179(7)	$^3/_8$,$^2/_8$,$^3/_8$
O1	0.4474(4)	0.0167(4)	0.9533(2)	0.0193(9)	1

[a] $a = 5.60398(3)$, $c = 13.93081(9)$ Å, space group *R3c*. $wR_p = 7.67$, $\chi^2 = 1.44$ (Neutron–HRPD beamline); $wR_p = 8.34$, $\chi^2 = 3.20$. (XRD Panalytical) [b] O1 U_{ij} parameters: $U_{11} = 0.021(1)$, $U_{22} = 0.019(1)$, $U_{33} = 0.019(1)$, $U_{12} = 0.007(1)$, $U_{13} = -0.004(1)$, $U_{23} = -0.007(1)$. The quoted O U_{iso} is an equivalent value derived from these ADPs.

(ca. $1 \times 10^{-8}\ \Omega^{-1}\,cm^{-1}$ for $BiTi_{3/8}Fe_{2/8}Mg_{3/8}O_3$ versus ca. $1 \times 10^{-4}\ \Omega^{-1}\,cm^{-1}$ for $BiTi_{3/8}Fe_{2/8}Ni_{3/8}O_3$ as measured at 400 K).

Dielectric permittivity measured at 1 MHz for the $BiTi_{3/8}Fe_{2/8}Mg_{3/8}O_3$ composition is shown in Figure 3. The sharp peak in permittivity at approximately 730 °C is characteristic

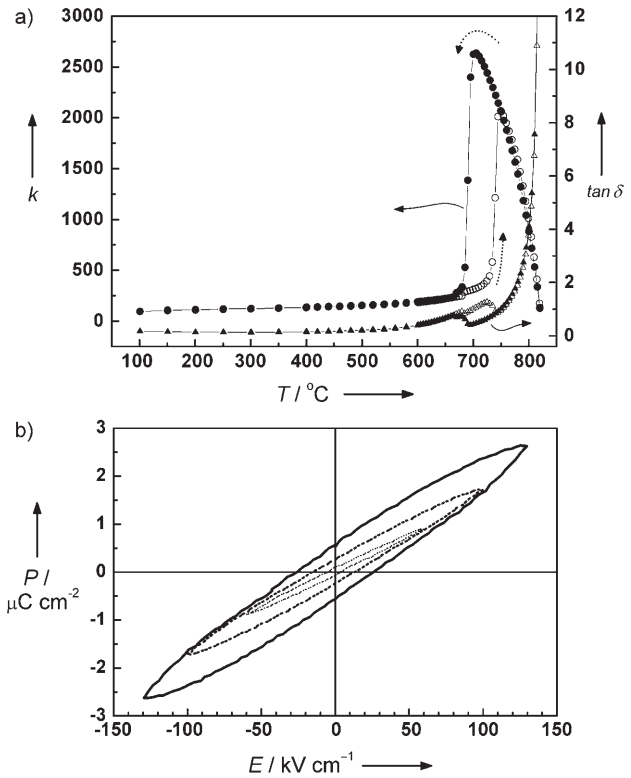

Figure 3. a) Temperature dependence of the relative permittivity (○,●, left axis) and dielectric loss (▲,△, right axis) measured at 1 MHz for $BiTi_{3/8}Fe_{2/8}Mg_{3/8}O_3$. Open data points represent data collected on heating; closed points represent data collected on cooling. At 100 °C, $\tan\delta = 0.20$ (measured value). b) Hysteresis loops of polarization versus applied electric field measured for increasing maximum applied fields on bulk $BiTi_{3/8}Fe_{2/8}Mg_{3/8}O_3$ at room temperature.

of a ferroelectric Curie temperature (T_C) transition to a nonpolar high-temperature structure. High-temperature powder neutron diffraction data collected at 740 °C confirm the presence of a cubic perovskite, which was refined in the space group $Pm\bar{3}m$ (Figure S7 in the Supporting Information). Data collected while cooling from 740 °C show a mixed-phase region from 685 °C to 675 °C as well as a rapid increase in volume upon formation of the *R3c* phase, thus supporting the characterization of this transition as first-order and matching the hysteresis in the permittivity. (Figure S8 in the Supporting Information). Dielectric loss (right axis of Figure 3) remains quite low (less than one) up to T_C, reflecting the low conductivity of the Mg^{2+}-containing material. Permittivity data from the more conductive $BiTi_{3/8}Fe_{2/8}Ni_{3/8}O_3$ composition (Figure S9 in the Supporting Information) are dominated by high loss tangent values.

Ferroelectric hysteresis loops of polarization versus applied electric field measured at 25 °C on thin (0.3 mm thick), polished pellets of $BiTi_{3/8}Fe_{2/8}Mg_{3/8}O_3$ are shown in Figure 3b. With increasing maximum applied field, the measured remanent polarization (P_r) and coercivity (E_c) increased as the loop expanded. No indication of room-temperature loop saturation was observed at the highest applied fields; given the very high T_C of $BiTi_{3/8}Fe_{2/8}Mg_{3/8}O_3$, this finding is not surprising. Although the measured remanent polarization was quite small (ca. 0.5 $\mu C\,cm^{-2}$), it clearly demonstrates the switchable polar ferroelectric structure of $BiTi_{3/8}Fe_{2/8}Mg_{3/8}O_3$. These hysteresis loops are very similar to that reported for initial studies on $BiFeO_3$.[14] Only recently, with improved processing and doping substitutions, have more substantial ferroelectric hysteresis loops been observed in $BiFeO_3$.[15]

Considering distortions from the $Pm\bar{3}m$ structure of the simple cubic perovskite, the F_R *R3c* structure arises from ferroelectric Bi-cation displacements along $[111]_p$ (the subscript p refers to the simple cubic perovskite unit cell) to give *R3m* symmetry with subsequent $a^-a^-a^-$ tilts about $[111]_p$, thus producing *R3c* symmetry. Further symmetry lowering to *Cc* can be driven by a change in tilt system to $a^-a^-c^-$ and also by a change in polarization direction from $[111]_p$ to $[hhl]_p$ owing to A- and B-site displacement. The mean octahedral tilts $\langle\omega\rangle$ about $[111]_p$ of $BiTi_{3/8}Fe_{2/8}Mg_{3/8}O_3$ (11.94°) and $BiTi_{3/8}Fe_{2/8}Ni_{3/8}O_3$ (12.21°) are nearly identical to that of $BiFeO_3$ (12.2°), while that of F_R $PbZr_{0.53}Ti_{0.47}O_3$ (1.4°) is significantly smaller (Table S2 in the Supporting Information).[16]

For $BiTi_{3/8}Fe_{2/8}Ni_{3/8}O_3$, the displacement of the Bi^{3+} ion from the centroid of the oxide cuboctahedron (0.62 Å) is smaller than that in $BiFeO_3$ (0.67 Å), while that for $BiTi_{3/8}Fe_{2/8}Mg_{3/8}O_3$ (0.66 Å) is nearly identical to $BiFeO_3$. Both $BiTi_{3/8}Fe_{2/8}Mg_{3/8}O_3$ and $BiTi_{3/8}Fe_{2/8}Ni_{3/8}O_3$ differ from $BiFeO_3$ owing to the local displacement away from the threefold axis.[12] The resulting Bi coordination environment has three closest Bi–O contacts resulting from the $[111]_p$ displacement towards a triangular face of the cuboctahedron of oxide anions surrounding the A site (Figure 1a). The off-axis local displacement produces a fourth short Bi–O contact (2.440(5) Å) to an oxygen atom from a cuboctahedron square face that shares an edge with the triangular face towards which the $[111]_p$ cation displacement occurs. The three initially equivalent short bonds in $BiTi_{3/8}Fe_{2/8}Mg_{3/8}O_3$ relax locally to 2.242(3), 2.282(2), and 2.369(4) Å (Figure 1a). Four close Pb–O contacts are found in both F_R and F_T phases of PZT, for which pair distribution function and theoretical work indicate that three-coordination is strongly disfavored.[17] In this case, the direction of the Bi-cation displacement from $[111]_p$ is along the pseudocubic $\langle 110\rangle_p$ directions

towards the fourth oxide neighbor, in contrast to F_R-PZT, for which displacements perpendicular to $[111]_p$ (which condense to give the monoclinic phases observed at the MPB) occur along $\langle 100\rangle_p$.

The B site is displaced along $[111]_p$ towards a triangular face of the octahedron to maximize its distance from the A cation that is displaced towards the opposite face (see Figure 1b and Figure S10 in the Supporting Information), giving average bond lengths of $3\times1.960(3)$ and $3\times2.110(3)$ Å. The local strain associated with the coexistence of three cations with very distinct bonding requirements on the octahedral site is evident in the bond valence sums (Table 3), which show underbonding for Ti^{4+} and overbonding for Ni^{2+} and Mg^{2+}, thus suggesting that the refined average structure contains considerable local distortions. The more severe underbonding and overbonding in the Mg^{2+} species gives rise to greater anisotropic broadening (Figure S11 in the Supporting Information) and a larger B-site displacement parameter.

Table 3: Bond lengths and bond valence sums for $BiTi_{3/8}Fe_{2/8}Ni_{3/8}O_3$ (left) and $BiTi_{3/8}Fe_{2/8}Mg_{3/8}O_3$ (right).

Bond	Bond length (Å)	Bond	Bond length (Å)
Bi–O1	2.258(1), 2.299(1)	Bi–O1	2.242(3), 2.282(2)
	2.391(1), 2.408(2)		2.369(4), 2.440(5)
	2.575(1), 2.581(1)		2.598(3), 2.604(3)
	3.142(1), 3.147(1)		3.156(3), 3.161(2)
	3.313(2), 3.340(1)		3.319(5), 3.401(3)
	3.372(1), 3.439(1)		3.432(2), 3.495(3)
BVS_{Bi}[a]	2.88	BVS_{Bi}[a]	2.88
M–O1	$3\times1.959(1)$	M–O1	$3\times1.960(3)$
	$3\times2.089(1)$		$3\times2.110(3)$
$BVS_{Ti,Fe,Ni}$	3.46,2.98,2.24	$BVS_{Ti,Fe,Mg}$	3.38,2.90,2.43
$BVS_{Ave\ M}$	2.88	$BVS_{Ave\ M}$	2.90
BVS_O	1.92	BVS_O	1.93

[a] Bond valence sums (BVS) are given in valence units (v.u.). The average BVS listed for the transition metal site (M) is weighted by the fractional occupancy. M = Ti^{4+}, Fe^{3+}, or Ni^{2+}/Mg^{2+}.

$BiTi_{3/8}Fe_{2/8}Mg_{3/8}O_3$ is a solid solution of $BiMg_{1/2}Ti_{1/2}O_3$ (an antiferroelectric (AFE) material that is isostructural with $PbZrO_3$ and can only be synthesized at high pressure)[18] and the rhombohedral ferroelectric material $BiFeO_3$. Despite being much closer in composition to the metastable $BiMg_{1/2}Ti_{1/2}O_3$, $BiTi_{3/8}Fe_{2/8}Mg_{3/8}O_3$ adopts an F_R structure related to that of $BiFeO_3$ and can be synthesized at ambient pressure. This finding is unusual crystal chemistry and cannot be understood simply as a transition to a stabilized doped $BiFeO_3$, owing to the low Fe^{3+} content (25%), the enhanced thermal stability ($BiFeO_3$ decomposes at the temperatures of ca. 950 °C used for synthesis in this study),[19] and the differences in structure reflected in the disordered A-site displacements (which produce a four-coordinate environment reminiscent of those in F_M- and F_R-PZT). The B-site ionic sizes and tolerance factors of $BiFeO_3$ ($t = 0.956$) and $BiMg_{1/2}Ti_{1/2}O_3$ ($t = 0.948$) are very similar, suggesting that specific bonding factors stabilize $BiTi_{3/8}Fe_{2/8}Mg_{3/8}O_3$ and $BiTi_{3/8}Fe_{2/8}Ni_{3/8}O_3$. Fe^{3+} ions can adopt a range of low-symmetry coordination environments owing to the $3d^5$ configuration, in contrast to Mg^{2+} ions, which disfavor low-symmetry environments because of the absence of valence-shell d orbitals. This situation stabilizes $[111]_p$ B-cation displacements and thus favors correlated A-site displacement in the same direction, thereby driving the transition from AFE $BiMg_{1/2}Ti_{1/2}O_3$ in which A-cation displacements are predominantly along $\langle 110\rangle_p$ to an F_R phase with $[111]_p$ displacements of both A and B cations. The preferred four close A–O contacts are achieved by superimposing a locally disordered $\langle 110\rangle_p$ displacement, which survives from $BiMg_{1/2}Ti_{1/2}O_3$ and can operate with $\langle 100\rangle_p$ A-site displacements favored by Ti to contribute to the $[111]_p$ polarization. This combination of A-site displacements driven by occupancy of B sites by different cations is found in the stabilization of the F_R-PZT phase by the introduction of Ti (which produces predominant $\langle 100\rangle_p$ A-site displacements) into AFE $PbZrO_3$ with its $\langle 110\rangle_p$ A-site displacements.[17]

Bismuth on the A site of the perovskite structure is rare, but in this case it is stabilized in a new polar phase by the synergy of the different bonding requirements of the three B-site cations with those of the Bi^{3+} ion. The structural flexibility of Fe^{3+} and Ti^{4+} ions enables optimization of the Bi–O environment by compensating for the less diverse structural chemistry of Mg^{2+} and Ni^{2+} ions. The use of enhanced chemical diversity to generate islands of stability in the energy landscape[20] may allow access to important structure types other than perovskite under apparently unfavorable circumstances.[21]

Received: July 13, 2007
Published online: October 11, 2007

Keywords: bismuth · ferroelectric materials · neutron diffraction · perovskite phases · polarity

[1] G. H. Haertling, *J. Am. Ceram. Soc.* **1999**, *82*, 797.
[2] B. Noheda, D. E. Cox, *Phase Transitions* **2006**, *79*, 5.
[3] P. Baettig, C. F. Schelle, R. LeSar, U. V. Waghmare, N. A. Spaldin, *Chem. Mater.* **2005**, *17*, 1376.
[4] H. Yan, H. Zhang, R. Ubic, M. J. Reece, J. Liu, Z. Shen, Z. Zhang, *Adv. Mater.* **2005**, *17*, 1261.
[5] Y. Saito, H. Takao, T. Tani, T. Nonoyama, K. Takatori, T. Homma, T. Nagaya, M. Nakamura, *Nature* **2004**, *432*, 84.
[6] R. E. Eitel, C. A. Randall, T. R. Shrout, P. W. Rehrig, W. Hackenberger, S.-E. Park, *Jpn. J. Appl. Phys. Part 1* **2001**, *40*, 5999.
[7] V. S. Filip'ev, N. P. Smolyaninov, E. G. Fesenko, I. N. Belyaev, *Kristallografiya* **1960**, *5*, 958.
[8] H. Hughes, M. Allix, C. A. Bridges, J. B. Claridge, X. Kuang, H. Niu, S. Taylor, W. Song, M. J. Rosseinsky, *J. Am. Chem. Soc.* **2005**, *127*, 13790.
[9] T. Atou, H. Chiba, K. Ohoyama, Y. Yamaguchi, Y. Syono, *J. Solid State Chem.* **1999**, *145*, 639.
[10] S. Ishiwata, M. Azuma, M. Takano, E. Nishibori, M. Takata, M. Sakata, K. Kato, *J. Mater. Chem.* **2002**, *12*, 3733.
[11] A. A. Belik, S. Iikubo, T. Yokosawa, K. Kodama, N. Igawa, S. Shamoto, M. Azuma, M. Takano, K. Kimoto, Y. Matsui, E. Takayama-Muromachi, *J. Am. Chem. Soc.* **2007**, *129*, 971.
[12] F. Kubel, H. Schmid, *Acta Crystallogr. Sect. B* **1990**, *46*, 698.
[13] D. L. Corker, A. M. Glazer, R. W. Whatmore, A. Stallard, F. Fauth, *J. Phys. Condens. Matter* **1998**, *10*, 6251.

[14] J. R. Teague, R. Gerson, W. J. James, *Solid State Commun.* **1970**, *8*, 1073.
[15] Y. P. Wang, L. Zhou, M. F. Zhang, X. Y. Chen, J.-M. Liu, Z. G. Liu, *Appl. Phys. Lett.* **2004**, *84*, 1731.
[16] N. W. Thomas, A. Beitollahi, *Acta Crystallogr. Sect. B* **1994**, *50*, 549.
[17] I. Grinberg, V. R. Cooper, A. M. Rappe, *Phys. Rev. B* **2004**, *69*, 144118.
[18] D. D. Khalyavin, A. N. Salak, N. P. Vyshatko, A. B. Lopes, N. M. Olekhnovich, A. V. Pushkarev, I. I. Maroz, Y. V. Radyush, *Chem. Mater.* **2006**, *18*, 5104.
[19] M. I. Morozov, N. A. Lomanova, V. V. Gusarov, *Russ. J. Gen. Chem.* **2003**, *73*, 1676.
[20] J. C. Schön, M. A. C. Wevers, M. Jansen, *J. Phys. Condens. Matter* **2003**, *15*, 5479.
[21] D. A. van der Griend, K. R. Poeppelmeier, *Int. J. Inorg. Mater.* **2001**, *3*, 1277.

